JOURNAL OF CATALYSIS 144, 525–543 (1993)

CO-Induced Morphological Changes of Rh Crystallites: Mechanisms, Kinetics, and Real-Space Imaging on the Atomic Scale

N. KRUSE AND A. GAUSSMANN

Technisch Chemisches Labor, ETH Zentrum, CH 8092 Zürich, Switzerland

Received April 2, 1993; revised July 12, 1993

The reaction of CO with Rh crystals of almost hemispherical shape (field emitter tips) was studied at various temperatures between 200 and 420 K and at pressures up to 10^{-1} Pa. Strong morphological changes of the crystals could be observed with atomic resolution by field ion microscopy (FIM). After field-free reaction with CO at 360 and 420 K the hemispherical Rh crystals appeared to be transformed into polyhedral shapes. High-index surface planes were absent on these crystals, i.e., kink sites were largely used up in faceting. More generally, the morphology of the reshaped crystals contained mainly planes with {001}, {011}, {111}, and {113} symmetry. The CO-induced restructuring was found to be thermally activated: atomic displacements were first observed at a reaction temperature of 240 K but were absent at 200 K. Using (atom-probe) pulsed field desorption mass spectrometry (PFDMS), the underlying reaction mechanisms and kinetics were studied in small selected surface areas containing about 150 atomic sites. Besides CO the surface layer always contained Rh-subcarbonyls, $Rh^0(CO)_x$ ($x = 1$–3). Time-resolved measurements (reaction times between 0.5 ms and 0.1 s) revealed temperature-dependent delay times for $Rh^0(CO)_2$ formation. This observation could be consistently interpreted on the basis of a reaction model leading to the liberation of mobile, adsorbed $Rh^0(CO)_2$ after Rh–Rh bond breaking in kink site positions. More generally, the structural changes of Rh crystals observed in FIM were most likely caused by (thermally activated) $Rh^0(CO)_2$ formation and decomposition at kinks with intermediate diffusion across the surface. The results of the present study suggest $Rh^0(CO)_2$ to be the likely precursor species for $Rh^I(CO)_2$ formation as observed in studies with Rh/Al_2O_3 model catalysts.

INTRODUCTION

One of the ultimate goals in the application of surface science to fundamental catalytic research is the identification of intermediates during an ongoing reaction on a catalyst particle while characterizing the atomic structure of the particle surface at the same time. The invention of scanning tunneling and atomic force microscopy (STM and AFM) has led to the widespread opinion that the essential experimental basis for reaching this goal has now been laid. In fact, during the past few years a great deal of information has been gained about the atomic-scale structure of surfaces. For example, STM studies with metal single crystals have made visible various adsorbate-driven surface reconstructions or well-ordered adsorbate layers. The identification of transient species with unknown chemical composition, however, is difficult, if not impossible, even when operating the microscope in the spectroscopic mode.

STM and AFM studies with more realistic models of catalyst surfaces are still rather scarce. Recent attempts to image small supported metal clusters with atomic resolution were partly successful (*1–4*). Some progress was also made in determining morphologies of catalyst particles prepared by impregnation from a precursor solution on conducting supports (*5*). It appears, however, that atomic-scale information about surfaces of three-dimensional particles, say larger than ~2 nm, cannot be easily obtained by STM or AFM. Thus, at present there are drawbacks in the application of these methods to the structural characterization of catalyst particles, in particular, if one is interested

0021-9517/93 $5.00

in observing adsorbate-induced crystal reshaping along with reconstructions of particular surface planes.

With this background other experimental techniques have gained significance in providing microstructural information. Important contributions to this field were made by transmission electron microscopy. For example, changes in the morphology of supported catalyst particles due to heat treatment or chemical reaction, occasionally leading to the disruption of the particles, were made visible (*6*). Even *in situ* studies of dynamic processes on the atomic scale were performed (*7*). Modern TEM can be combined with X-ray microanalysis or electron energy loss spectroscopy, there are, however, conceptual and technical restrictions which do not allow the identification of chemical species under reaction conditions on a crystal surface well-defined in its atomic structure.

Another method capable of providing ultimate structural information is field ion microscopy (FIM). One of the advantages of this technique is that the sample is given in the form of a near hemisphere ("field emitter tip") with a radius of curvature of some ten nanometers. Thus, a tip can be considered a model of a single catalyst grain in the absence of any insulating support material. Early FIM work brought forth partly ambiguous results (*8, 9*) and it was argued that structural damage to the samples may be caused by the imaging process in high electric fields (*10–15*). Recently, however, it was shown that safe conclusions can be drawn and that adsorbate-induced reconstructions of single crystal planes can be viewed with atomic resolution (*16, 17*). On the one hand, the stringent vacuum conditions maintained during imaging impose restrictions to applications in heterogeneous catalysis. On the other hand, however, the combination of FIM with atom-probe techniques like pulsed field desorption mass spectrometry (PFDMS) provides a unique tool for the study of surface chemical reactions in a time-resolved manner and at the atomic scale. In a number of recent applications the high potential of PFDMS to elucidate reaction mechanisms and kinetics was demonstrated (*18–20*).

In the present paper results are presented that were obtained from studies of the CO interaction with Rh field emitter tips at temperatures up to 450 K. FIM was applied to reveal strong morphological changes transforming crystal shapes from nearly hemispherical into polyhedral. The chemical analysis of the adsorbed layer by PFDMS has identified Rh-subcarbonyl species, $Rh^0(CO)_x$ (x = 2,3), as mobile entities most likely involved in the restructuring processes. Some of the data were previously published in short communications (*17, 21*). A full account of the work is given here.

EXPERIMENTAL

Two different setups were used for the studies reported in this paper. Both were described in detail elsewhere (*19, 22, 23*). Thus, only a brief outline will be given here. The atomic structure of Rh tips before and after reaction with CO was determined in an all-metal field ion microscope equipped with a channel plate (ϕ = 3 in.) for image intensification. Field ionisation was continuously monitored by means of a video recording system. Individual micrographs presented below were taken by a camera. Field electron microscopy (FEM) was performed at reversed polarity before and after FIM. Samples were mounted on a four-pin holder which could be plugged into a fellow at the end of a magnetically coupled rod. Temperatures were measured by a thermocouple attached to the shank of the tip and connected to one pair of the pin holder.

The rod allows for a rapid sample transfer under ultrahigh-vacuum (UHV) conditions between the microscope and a reaction chamber. In order to follow product formation during catalytic reactions, differentially pumped quadrupole mass spectrometers are attached to both chambers. The reaction chamber can be operated at pressures up to $2 \times 10^{+5}$ Pa. The residual gas pressures are always below 5×10^{-9} Pa in the FIM

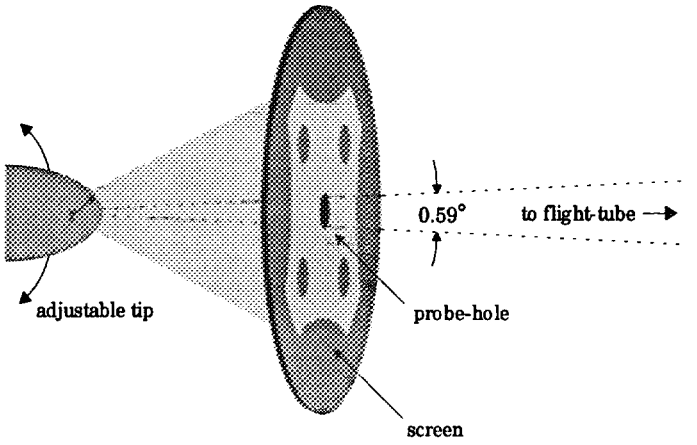

FIG. 1. Scheme of the experimental setup for pulsed field desorption mass spectrometry (atom-probe).

chamber and $\sim 10^{-7}$ Pa in the reaction chamber. The low-pressure studies (up to $\sim 10^{-1}$ Pa) reported here were conducted in the microscope.

Strictly field-free conditions were maintained during the reaction experiments. After field ion imaging of the clean tip surfaces, the voltages were switched off before introducing the CO gas and adjusting the reaction temperature. At the end of a reaction experiment the sample was cooled to cryogenic temperatures before removing the CO gas. Subsequently the sample was imaged in Ne.

Kinetic reaction studies were performed by PFDMS in another apparatus.

The basic principle of this method is to apply high electric field strengths $F < 50$ V/nm in form of short field pulses (widths > 100 ns, repetition rates < 100 kHz) to a counter electrode (with a hole), mounted at a distance of 0.1 mm in front of a Rh sample. This leads to the desorption of adsorbed species in form of ions which are separated and detected in a time-of-flight mass spectrometer. Thus, conclusions about the composition of the adsorbed layer can be drawn. As shown in Fig. 1, a screen with a probe-hole is mounted at the entrance of the flight tube. By tilting the Rh tip in front of the hole, crystallographically different planes with up to ~250 atomic sites (the size of the monitored area can be adjusted by means of electron lenses, but depends also on the radius of curvature of the tip which is determined from the calibrated onset voltage for krypton field ionisation) can be probed. The selection of a particular surface area is usually controlled in a separate experiment by FEM at reversed polarity. Gas pressures were measured by means of a spinning rotor viscosity gauge (Leybold Heraeus VM212).

In the time t_R, between the pulses, an arbitrary dc field F_{dc} can be maintained. For the measurements to be reported here, a dc field was not applied. Kinetic data of surface reactions can be obtained as schematically illustrated in Fig. 2. While continuously dosing the sample surface by CO, adsorption takes place only in the time interval, t_R, between two field pulses. At the end of t_R, the adsorbed layer is desorbed by a field pulse. If the pulse field strength ${}_1F_{P_1}$ is high enough, the ion intensity is a measure of the species' concentration on the surface (provided, the influence of fragmentation and association is known as, for example, from dc field strength variation). Under these conditions the beginning of each reaction period is characterized by a zero adsorbate concentration. The longer t_R becomes, the more the adsorption process proceeds. As the surface layer builds up, consecutive chemical reactions become possible. Thus, by systematically varying t_R, the kinetics of these processes can be monitored. This is normally

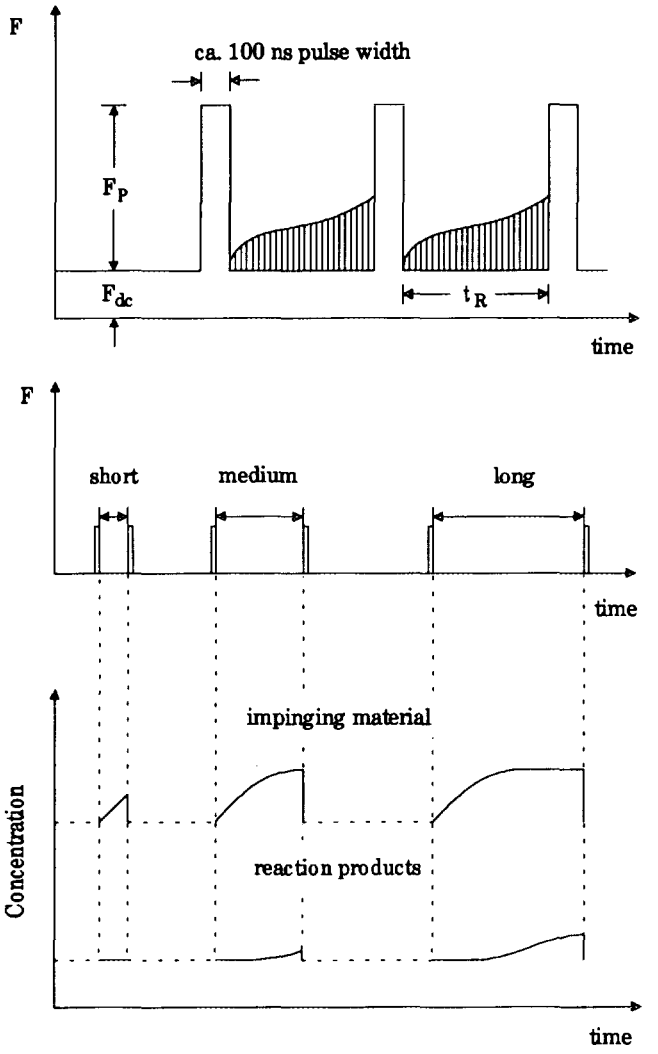

FIG. 2. Schematic diagram of field pulses with various repetition rates analyzing the formation of reaction intermediates and products.

done in the range between 100 μs and several seconds.

Rh field emitter tips were prepared by electrochemical etching in a molten mixture (1 : 4 w/w) of NaCl and $NaNO_3$. The tips were cleaned in UHV by cycles of either field evaporation and Ne-sputtering (for FIM) or field evaporation and heating in hydrogen/oxygen (for PFDMS). The CO gas used in the reaction studies preceding FIM was purified by freezing out contaminations in a molecular sieve cooled by liquid nitrogen (the partial pressure of CO at 78 K is in the range of some 10^{+2} Pa). Research grade CO (99.997%) was employed in PFDMS.

RESULTS

Field Ion Microscopy

In this part of the paper we present FIM results which provide evidence that the morphology of Rh field emitter tips changes during their reaction with CO. In order to differentiate between purely thermal and chemical effects, blank runs were made by heating several Rh specimens to tempera-

tures between 400 and 500 K in the absence of gaseous CO.

Figure 3a shows a micrograph of a (111)-oriented Rh tip cleaned according to the procedure described above. Imaging was performed in Ne at 94 K and at 37 V/nm. An average tip radius, $r = 18$ nm, can be determined from net plane counting. For this radius a considerable number of different surface planes, both low and high index, are clearly developed. For better orientation, a schematic sterographic projection (ignoring true angles and distances) is shown in Fig. 3b. Stepped planes like {113} and {011} are located along the ⟨110⟩ zone lines connecting the central (111) pole with the peripherical {111} and {001} poles. {133} planes, though smaller, are present between {111} and {011}. Six {012} planes are also clearly visible and located along the ⟨211⟩ zone lines.

Heating the tip at 500 K for 1 min and subsequent imaging in Ne at 94 K and 33 V/nm resulted in the micrograph shown in Fig. 3c. A comparison with Fig. 3a reveals that atom displacements have taken place in certain areas of the sample surface. This may occasionally have caused reconstructions such as those occurring between (021) and (153) (see arrow). There is also no doubt that surface diffusion has led to some shrinkage in the topmost layers of small planes. Some of the very bright spots as, for example, on (201) or $(1\bar{1}1)$ are possibly associated with impurities either segregated from the bulk to the surface or adsorbed from the gas phase. Most importantly, however, there are neither changes in the overall tip morphology nor well-defined faceting of individual planes due to heating. This is a general result which also holds when heat-treating the sample during extended time periods or when using samples of orientation other than [111]. An increase of the field strength from 33 V/nm in Fig. 3c to 36 V/nm in Fig. 3d was found to cause field evaporation of less than one surface layer so that the original morphology of the Rh tip, imaged in Fig. 3a, reappeared.

In the following, we present FIM results of our experiments with CO. Reaction temperatures of 200, 300, 360, and 420 K were chosen. The starting point for each experiment was a clean (001)-oriented Rh sample, imaged at $F = 37$ V/nm. The shapes of the Rh field emitter tip before the reaction experiments with CO are shown in Figs. 4a–7a. The results obtained from measurements at 420 K are shown along with schematic stereographic projection in Fig. 7. The radii of curvature of the clean specimens are similar and vary between 20 nm in Fig. 4a and 27 nm in Fig. 7a. The transition regions leading from the central (001) plane along ⟨110⟩ and ⟨100⟩ to the peripherical {111} and, respectively, {110} planes are neatly divided up into high-index planes. The outermost {111} poles and a number of smaller stepped planes are not shown in the stereographic projection of Fig. 7. In particular, there are always {015}, {013}, {012}, and {023} planes connecting the (001) pole with the {011} planes along the ⟨100⟩ direction. Stepped {115}, {113}, and {112} planes are located between the (001) pole and {110} planes along ⟨110⟩. Other planes such as {135} and {133} along ⟨310⟩ or, respectively, {123} and {122} along ⟨100⟩ are also visible.

A number of important observations can be made by comparing the micrographs of the clean surfaces (Figs. 4a to 7a) with those obtained after reaction with CO (Figs. 4b to 7b). Similar experimental conditions concerning the reaction times and gas pressures (10 min at 10^{-3} Pa and 30 min 10^{-4} Pa) were applied in order to allow cross-comparisons revealing the influence of the different temperatures applied during the reaction studies. Subsequent field ion imaging of the samples in Ne was always performed at quite low field strengths so that the rings of atoms surrounding the low-index poles remain invisible. Of course, these rings could be revealed by further increasing the viewing field. Due to the onset of concomitant field desorption/field evaporation with consequent layer damage, the respective micrographs are not presented here.

Almost no topographic changes seem to have occurred during reaction with CO at 200 K. Additional small spots are observed

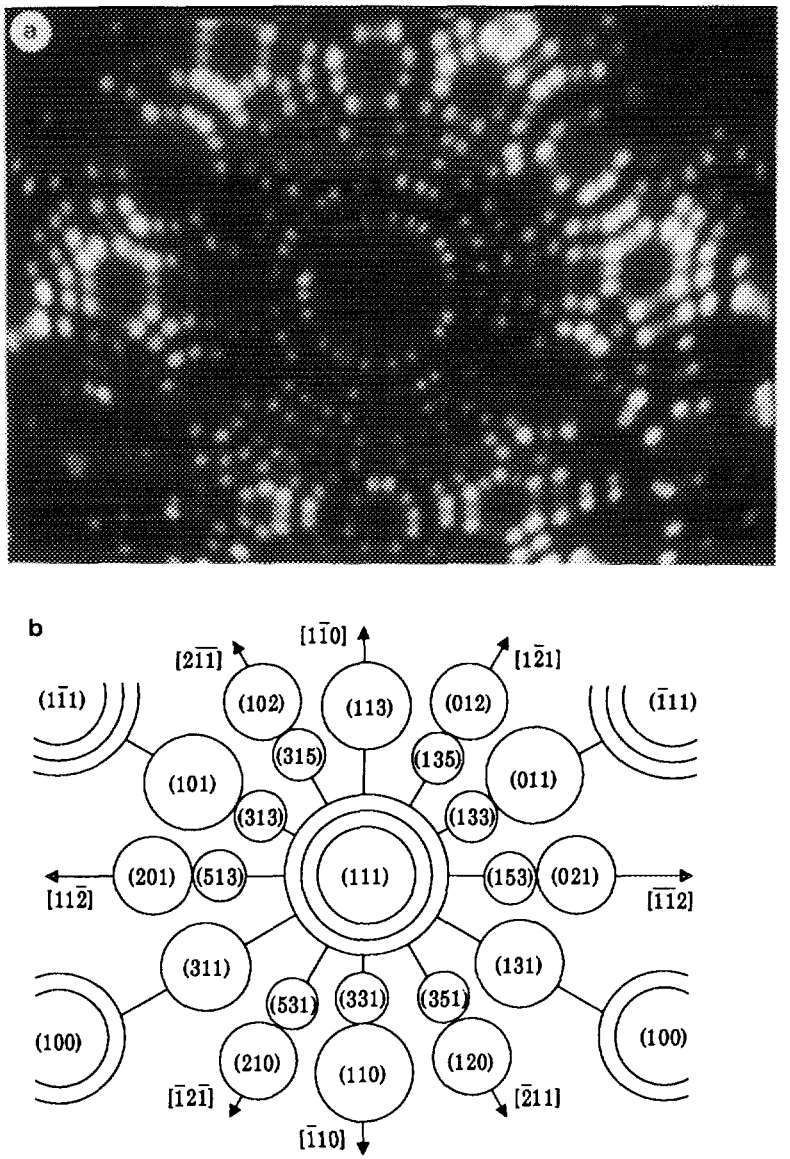

FIG. 3. Ne-field ion micrographs of a [111]-oriented Rh field emitter tip (a,c,d) along with a schematic stereographic projection (b) indicating surface planes and zone lines; experimental conditions are: (a) clean surface imaged at 94 K and $F \sim 37$ V/nm, (c) same Rh sample imaged at 94 K and $F \sim 33$ V/nm after heating at 500 K for 1 min under UHV-conditions, (d) same Rh sample imaged at 94 K and at increased field strength of F ~ 36 V/nm.

in the bright areas of {012} and its surroundings. They are most likely due to the presence of impurity species. The imaging field strength was ~24 V/nm, i.e., ~65% of the value used in Fig. 4a. Neither field desorption of chemisorbed CO nor field evaporation of Rh was seen under these conditions. Measurements with PFDMS have shown that at 298 K a field strength of at least 26 V/nm is necessary for these processes to occur (*19*). Interestingly, the image contrast in Fig. 4b is quite high so that some high-index planes appear with inner-plane resolution. Field ion imaging of Rh tips covered

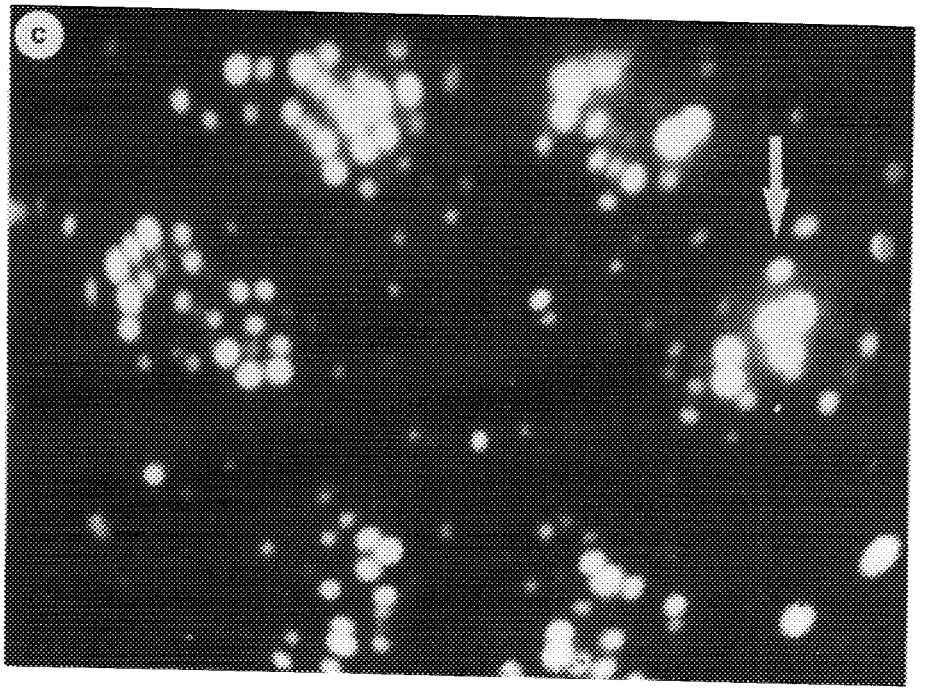

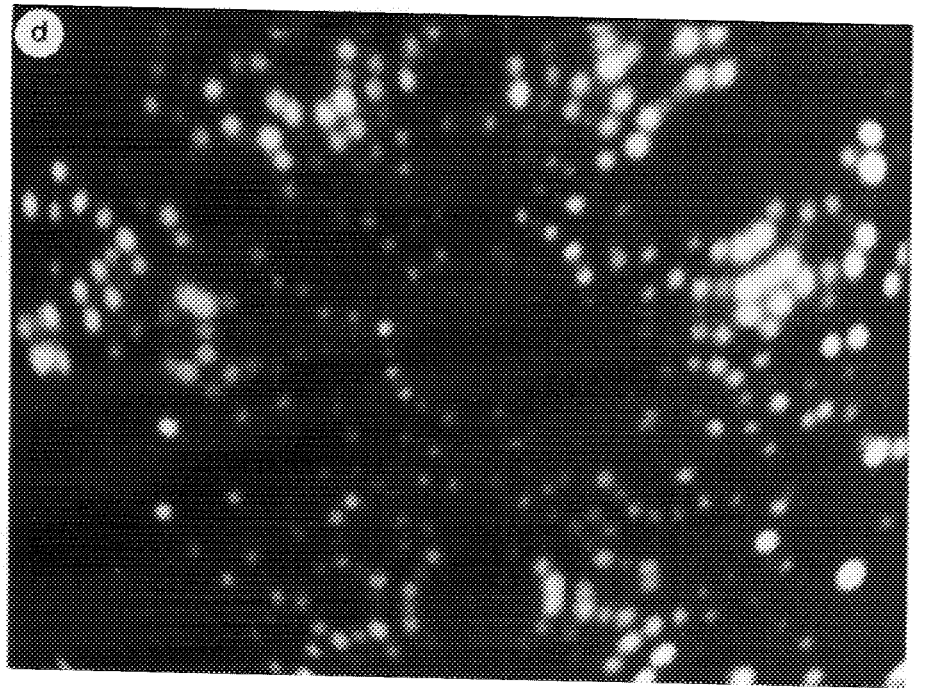

FIG. 3—*Continued*

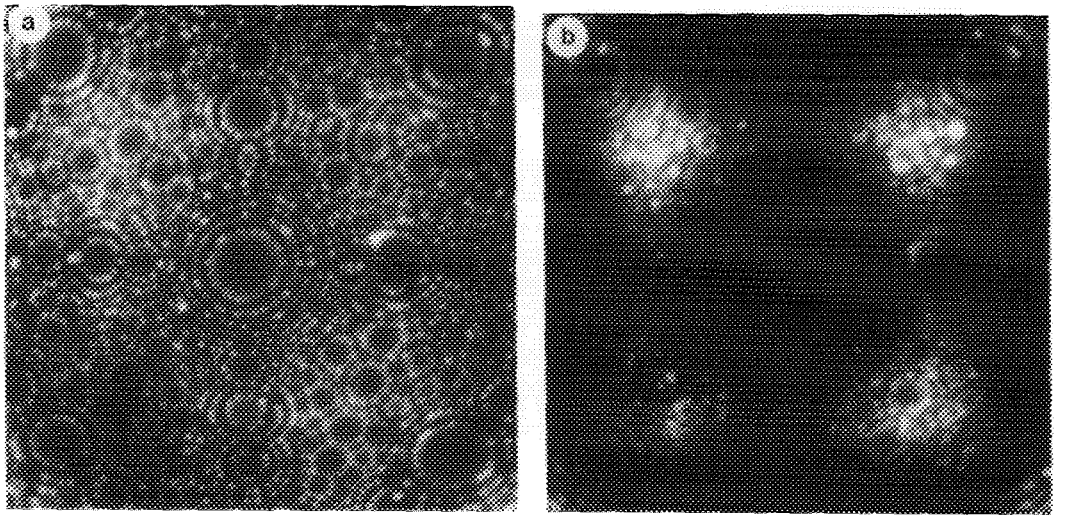

FIG. 4. Ne-field ion micrographs of a [001]-oriented Rh field emitter tip: (a) clean surface imaged at 85 K and $F \sim 37$ V/nm and (b) same sample imaged at 85 K and $F \sim 28$ V/nm after interaction with CO for 10 min at 200 K and 10^{-3} Pa.

by CO at temperatures below 200 K were also taken and revealed micrographs identical with those shown in Fig. 4.

Conspicuous structural changes of the Rh specimens seem to have taken place during the reaction with CO at higher temperatures. They are most clearly developed in Figs. 6b and 7b, i.e., after exposing the samples to CO at 360 and 420 K. Nevertheless, there is clear evidence that topographic changes in the sample surface take already place at 300 K. According to Fig. 5b, mainly the {012} and neighboring planes (e.g., {023}) are involved. Single atoms seem to be dis-

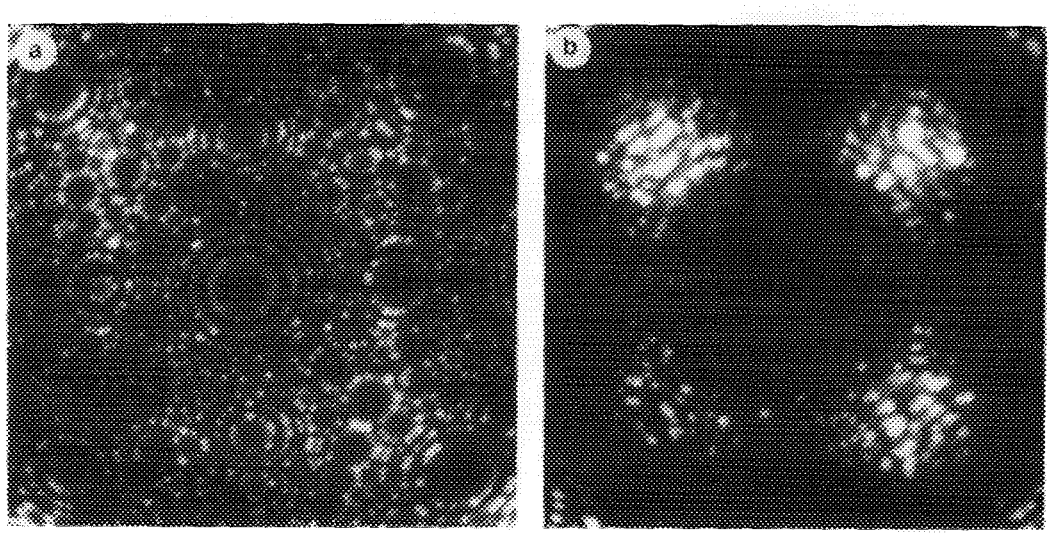

FIG. 5. Ne-field ion micrographs of a [001]-oriented Rh field emitter tip: (a) clean surface imaged at 85 K and $F \sim 37$ V/nm and (b) same sample imaged at 85 K and $F \sim 27$ V/nm after interaction with CO for 10 min at 300 K and 10^{-3} Pa.

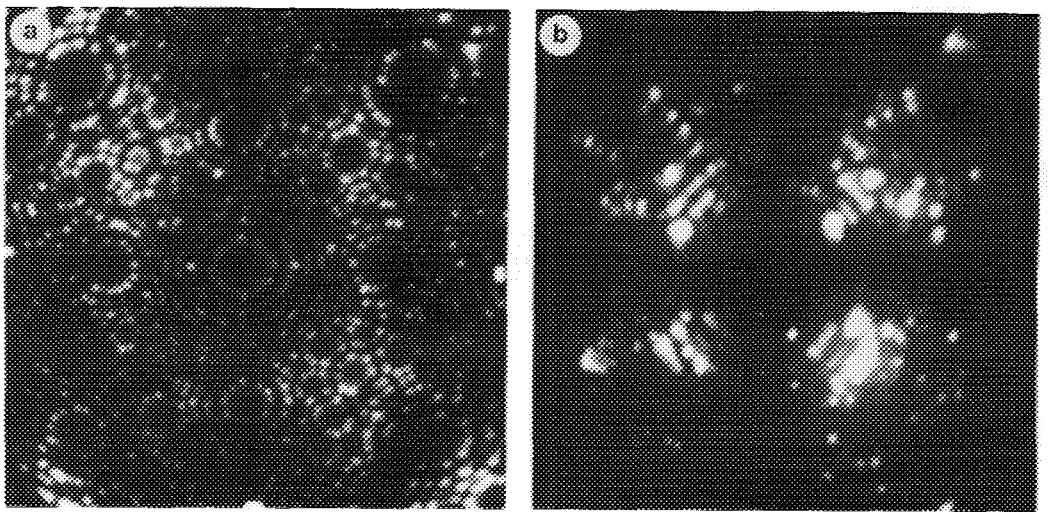

FIG. 6. Ne-field ion micrographs of a [001]-oriented Rh field emitter tip: (a) clean surface imaged at 85 K and $F \sim 37$ V/nm and (b) same sample imaged at 85 K and $F \sim 27$ V/nm after interaction with CO for 30 min at 360 K and 10^{-4} Pa.

placed from their original positions so that vacancies are left and new extra spots appear. Chains of atoms oriented perpendicular to the ⟨100⟩ zone lines are also observed. The number of net planes along ⟨100⟩ seem to be reduced, which is in accordance with the formation of facets.

After reaction with CO at 360 K, the structural features are more clearly developed. Planes such as {013} have now also undergone faceting. The terraces of the facets along the ⟨100⟩ zone lines are of {110} and {001} symmetry. This can be easily shown by using ball models. More generally, the morphology of the whole crystal consists of planes with {001}, {110}, {111}, and {113} symmetry.

The field strengths used for ion imaging after reaction at 300 and 360 K were quite low again, i.e., about 26 V/nm. A somewhat higher value, 28 V/nm, was used to reveal details of the CO-induced structural changes occurring at 420 K. Nevertheless, the respective micrograph shown in Fig. 7b was stable during minutes of imaging, with no spots either moving or disappearing. As compared to Fig. 7a the whole apex of the specimen seems now to be reshaped. The resulting morphology is visualized in the schematic stereographic projection at the bottom right of Fig. 7. Obviously, the original crystal shape is transformed from nearly hemispherical before reaction into polyhedral after reaction. This transformation is associated with a faceting of the high-index planes, most clearly visible for the vicinal planes of the (001) pole. As compared to the study at 360 K, the {113} planes seem to be smaller. On the other hand, the structural features of the {012} and its neighboring planes along the ⟨100⟩ zone lines are not as clearly discernible in Fig. 7b as in Fig. 6b. This is likely related to the presence of surface carbon (and oxygen) which can be more easily deposited by dissociation of chemisorbed CO at 420 K than at 360 K. In fact, it was shown recently that surface carbon can block the CO-induced reconstruction on {012} (*24*). Details are discussed below.

The polyhedral particle morphology imaged in Fig. 7b can be easily built up by ball models in order to illustrate the faceting of the slopes. The terraces of the facets contain planes of {001}, {110}, and {111} symmetry. Furthermore, it is seen that the bright spots

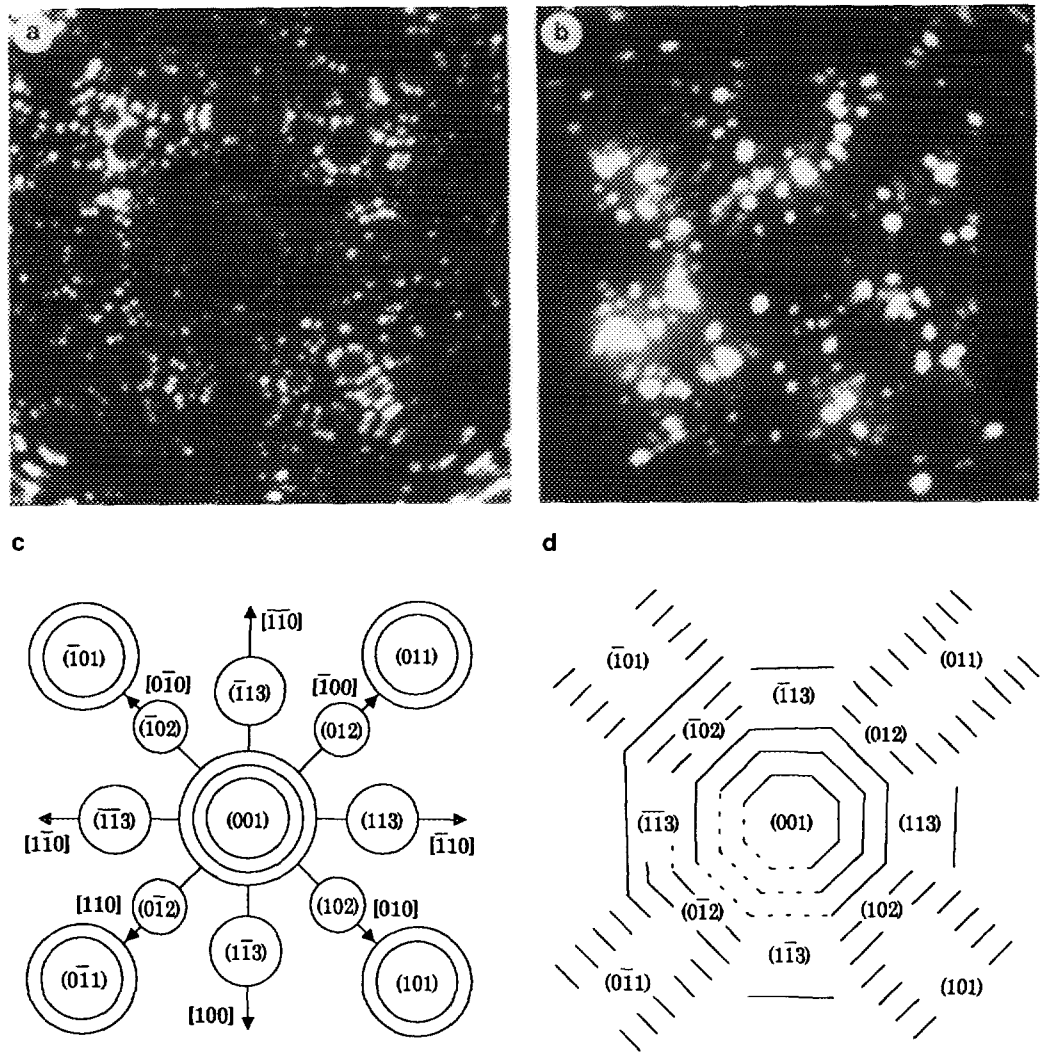

FIG. 7. Ne-field ion micrograph of a [001]-oriented Rh field emitter tip along with schematic stereographic projections indicating surface planes and zone lines of the Rh field emitter tip: (a) clean surface imaged at 85 K and $F \sim 37$ V/nm, (b) same Rh sample imaged at 85 K and $F \sim 29$ V/nm after interaction with CO for 30 min at 420 K and 10^{-4} Pa, (c) schematic stereographic projection of the clean sample, applying also to Figs. 4a, 5a, 6a, and (d) stereographic projection indicating morphological changes of the crystal along with faceting of crystallographic planes due to the reaction with CO.

present in Fig. 7b are located in the boundary regions between differently oriented slopes of the polyhedron. The brightness of the spots is due to the high local field strengths present in these strongly curved regions. When increasing the field strength slightly (by about 5%), the brightest spots disappeared first. Field evaporation became more intense at about 33 V/nm. Several Rh layers (exact counting is difficult as field evaporation occurs rather unregularly across the sample surface) had to be removed in order to restore the almost hemispherical shape of the apex.

The FIM results presented above have demonstrated that the CO-induced reshaping of the Rh specimens is thermally activated. Though detailed structural informa-

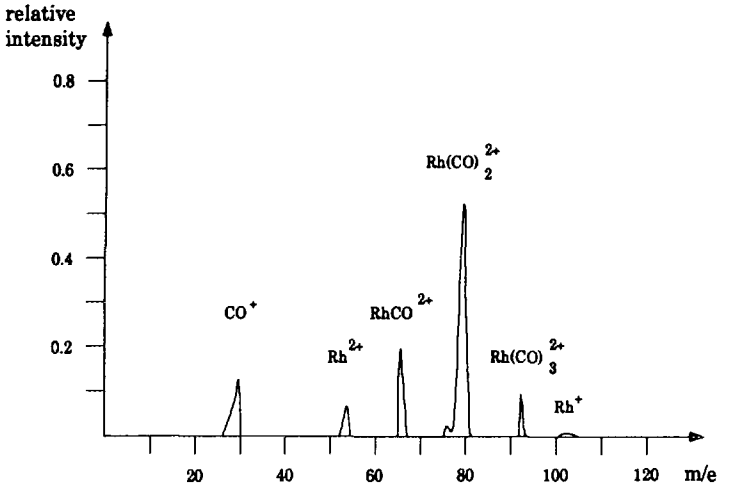

FIG. 8. Time-of-flight mass spectrum during reaction of CO with a Rh field emitter tip, obtained by probing a region of vicinal surfaces around the Rh (001) pole; monitored area: ~150 surface sites containing parts of the (013) plane; experimental conditions: T = 473 K, p_{CO} = 1.3 × 10^{-4} Pa, and field strength $F \sim 17$ V/nm.

tion was obtained in real-space with atomic resolution, no conclusions could be drawn on the underlying mechanisms and chemical processes.

Pulsed Field Desorption Mass Spectrometry

In this section we present results of our time-resolved reaction studies by PFDMS. Various regions of the tip apex were analyzed for their chemical composition during CO adsorption.

Figure 8 shows a typical time-of-flight mass spectrum obtained by probing about 150 surface atoms in the vicinity of the (001) pole of the tip. A previous check by field electron microscopy showed parts of the (013) plane to be contained in the monitored area. PFDMS was performed while CO was impinging on the surface at 1.3 × 10^{-4} Pa and 473 K. The desorption field strength was quite low, i.e., ~17 V/nm, during these measurements. Only pulses were applied, with no dc field, F_{dc}, being present during the reaction time, t_R = 0.5 ms. For $F_D <$ 26 V/nm, at 298 K, quantitative desorption of the adsorbed layer did not occur. This had been previously shown in elaborate studies on the field strength dependence of species desorption (*19*). Thus, a qualitative rather than a quantitative analysis of the surface layer was performed here. Small amounts desorbed by the field pulses were refilled during t_R so that a quasi steady adsorbate coverage was maintained.

Various ionic species are seen in the mass spectrum of Fig. 8. The respective intensities, plotted in relative numbers by relating to the total amount of material desorbed, were accumulated during 5 × 10^5 desorption cycles. Besides CO and the substrate material, Rh, subcarbonyls, RhCO, $Rh(CO)_2$, and $Rh(CO)_3$, appear in the mass spectrum as either singly or doubly charged ions. This result is interpreted in terms of a consecutive reaction taking place in the adsorbed layer and involving the respective neutral species. $RhCO^{2+}$ is understood as an ionic species resulting from field desorption of CO chemisorbed at steps, i.e., most probably at kinks, whereby the bonds between the respective Rh atom and its neighbours are broken. The high-index subcarbonyl species, $Rh(CO)_2$ and $Rh(CO)_3$, are formed by

subsequent addition of another one or two CO molecules to the respective Rh kink atom. Details of the $Rh(CO)_2$ formation kinetics can be deduced from reaction time variation measurements as described below. There is no indication that CO^+ and $RhCO^{2+}$ result from field fragmentation of adsorbed $Rh(CO)_{2,3}$ (*18*). Rh field evaporation, i.e., the removal of Rh lattice atoms in form of ions, is only of limited importance at F_D = 17 V/nm. Carbon and oxygen atoms released during the decomposition of the CO molecule are not desorbed at this low field strength.

Kinetic reaction studies cannot be performed at field strength values as low as those applied in Fig. 8. One of the prerequisites for these studies to become possible is that the field pulses lead to complete desorption of the adsorbed layer. As mentioned above, previous field strength variation measurements (*19*) indicated that a CO desorption probability of unity can only be obtained at field strengths higher than 26 V/nm (at 298 K). Under these conditions the sum of the $RhCO^{2+}$ and CO^+ ion intensities in terms of the number of ions per desorption pulse is a measure of the CO surface coverage built up during t_R. This is a quite general result obtained with a number of tips and probing crystallographically different areas. Variations, however, were seen in the relative amounts of $RhCO^{2+}$ and CO^+. More specifically, the intensities of both species could be reversed while keeping their sum constant. This is likely due to variations in the step densities within different monitored areas.

A point of particular interest is the formation of Rh-subcarbonyls. Due to their high ionisation probability these species dominate the mass spectrum in Fig. 8. On the other hand, it was found that in the "kinetic regime," i.e., at high field strengths, the reaction towards the $Rh(CO)_2$ stage is too slow to occur during t_R = 1 ms at 298 K (*25*). Thus, longer reaction times had to be chosen to reveal the onset as well as the progress of subcarbonyl formation. It had already been demonstrated that kinetic data are accessible in this manner (*25*). We now give a more complete account of these studies.

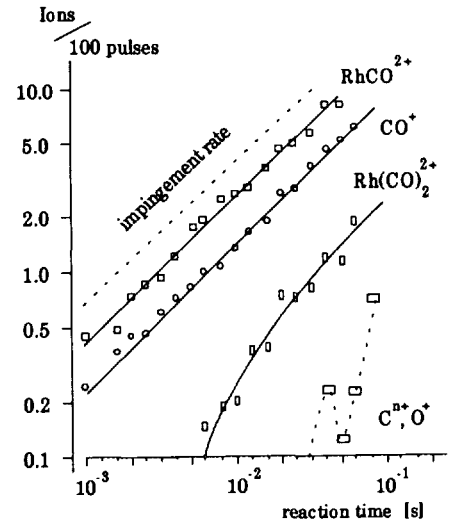

FIG. 9. Experimental intensities (ions per 100 pulses) as a function of the reaction time, t_R, monitored at ~150 surface sites with the probe-hole position as in Fig. 8; experimental conditions: T = 298 K, p_{CO} = 1.3 × 10^{-4} Pa, and high field strength, i.e., F ~ 28 V/nm.

In Fig. 9 the ion intensities of the various species are plotted for various reaction times between 1 ms and 0.1 s. Again, about 150 atoms close to the (001) pole, i.e., in a region containing the vicinal (013) plane, were probed during the reaction with CO at 1.3 × 10^{-4} Pa. However, the field strength was now as high as 28 V/nm, sufficient to ensure quantitative desorption by the field pulses at 298 K. Under these conditions adsorbed $Rh(CO)_3$ was only found in statistically insignificant amounts. They are omitted in Figs. 9 and 10.

There is a general trend in Fig. 9 in that the number of ions per desorption pulse (~surface coverage of the respective species) increases with extending reaction times. However, there are marked differences in the specific behavior of the various ionic species. It is seen that only $RhCO^{2+}$ and CO^+ are desorbed over the whole range

of reaction times. In contrast, $Rh(CO)_2^{2+}$ and C^{n+}/O^+ appear with delay times. Moreover, both $RhCO^{2+}$ and CO^+ intensities increase linearly with time whereas a higher order time dependence seems to apply for $Rh(CO)_2^{2+}$ and C^{n+}/O^+.

It has been argued above that $RhCO^{2+}$ and CO^+ are representative for chemisorbed CO. According to Fig. 9 the build-up of CO_{ad} proceeds with a constant rate, i.e., according to the simple Langmuir model. This is expected as the maximum coverages reached within the measured time scale are always considerably below the monolayer limit. Sticking probabilities can be derived by comparing the slope $d\theta_{CO}/dt$ with the impingement rate from the gas phase (the line marked "impingement rate" shows the expected ion current if all molecules impinging into the monitored surface area were measured, i.e., 100% sticking probability, no thermal desorption, no net diffusion supply or loss). Values of 0.85 . . . 0.95 are obtained which are somewhat larger than those determined for CO adsorption on a macroscopic (111)-oriented Rh single-crystal surface (*26*). This is most likely due to the presence of the many steps acting as trapping sites for impinging CO molecules.

In order to demonstrate more clearly that the field desorption rates of $Rh(CO)_2^{2+}$ and C^{n+}/O^+ depend on the reaction time, the ion intensities are replotted in terms of the number of ions per second in Fig. 10. The lowest intensity values entered into this figure are at the detection limit of the PFDMS instrument. The time lag in the formation of $Rh(CO)_2^{2+}$ is about 2 ms at 298 K. The desorption rate of this species increases until it reaches a constant level at long reaction times. This behaviour is a strong indication for $Rh(CO)_2$ being formed chemically during a consecutive surface reaction. It seems clear from the data that this reaction is more strongly dependent on the reaction time than would be expected for simple second order kinetics. As the intensities are quite low, we refrain from an evaluation of the respective rate law. Instead, direct comparison is made with measurements performed at somewhat higher temperature, i.e., 350 K. Though the number of data points is small, it is seen that the overall time behaviour of $Rh(CO)_2^{2+}$ desorption is similar to the one observed at 298 K. An important difference, however, is that this species now occurs with a shorter delay time. Thus, $Rh(CO)_2$ molecule formation is thermally activated. This result is consistent with the view that Rh–Rh bonds are broken during this process. Then, accordingly, $Rh(CO)_2$ would be field desorbed after its diffusion into the terrace layer.

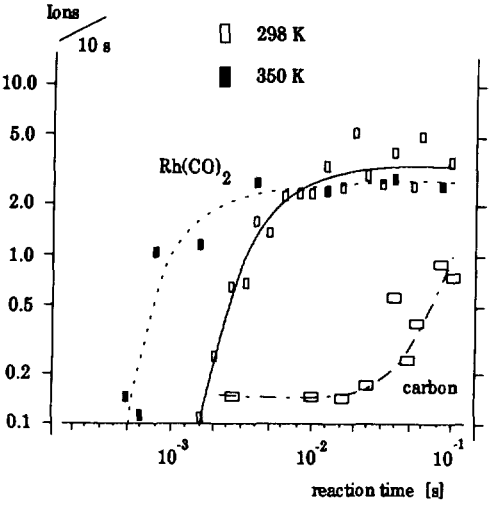

FIG. 10. Experimental intensities plotted in terms of the number of ions per 10 seconds as a function of the reaction times, t_R, with the same conditions as in Fig. 9 except for inclusion of a measurement at 350 K.

In Fig. 10, the field desorption rate of the C^{n+}/O^+ species increases at long reaction times. In fact, the behavior is similar to $Rh(CO)_2^{2+}$ at short reaction times, and it is most likely that both C^{n+} and O^+ ions originate from field desorption of adsorbed carbon and oxygen formed previously by chemical decomposition of CO_{ad}. This latter process does not follow simple first-order kinetics. It seems that a certain amount of CO_{ad} must be accumulated on the surface before decomposition begins. As the statistical significance of the measured ion intensities is not clear, fitting procedures, e.g.,

with a rate law $d\theta_C/dt \sim k\theta_{CO}^n$ have not been applied. In addition, field desorption of surface carbon is unlikely to be complete at $F = 28$ V/nm so that the coverages are higher than those reflected by the ion intensities. Possibly, accumulated carbon amounts inhibit the formation of $Rh(CO)_2$ as both decomposition and association necessitate step sites for their occurrence. This could explain why the $Rh(CO)_2^{2+}$ field desorption rate decreases with increasing reaction times. The temperature dependence of the C^{n+} intensities has as yet not been measured so that more detailed conclusions about the kinetics of the CO decomposition on stepped Rh surfaces cannot be drawn here.

PFDMS results very similar to those presented above were obtained by probing surface areas other than stepped (001). It must be concluded that the behavior of Rh field emitter crystals in reaction with CO is dominated by step sites which are always present no matter which specific area is monitored.

DISCUSSION

In the preceding section experimental evidence has been presented for the occurrence of CO-induced morphological changes of Rh field emitter particles. FIM has revealed the gross structural features of the particles as well as the detailed surface atomic arrangements. The remarkable finding of this study is the transformation of nearly hemispherical crystal particles into polyhedral shapes through reaction with adsorbed CO. A considerable mass transport must be assumed in order to understand this result. Time-resolved studies by PFDMS have clarified the transport mechanism and the associated reaction kinetics. Accordingly, a diffusion process is set into action through conversion of Rh kink site atoms into mobile, adsorbed $Rh^0(CO)_2$. Before proceeding to a more general discussion of these results, some arguments will be summarized which dispel concerns about misinterpretation of the data due to the application of the high-field experimental methods.

Field Effects

It was reported in early FIM work of O_2 or CO adsorption on W that layer damage occurs during ion imaging (*10–15*). Mechanisms advanced to explain this effect were based on electron impact during field ionization (*10, 12*) or energy transfer of "hot," i.e., polarized image gas atoms (*11*). In order to account for increasing surface disorder while imaging, gas-promoted displacement and desorption of substrate-adsorbate complex compounds was envisaged (*13–15*). In the present study the ion images were stable, i.e., spots neither moved nor disappeared at viewing fields of 26 V/nm. Thus, we conclude that the detailed Rh atomic arrangements were imaged as formed during the preceding field-free reaction experiments. However, it cannot be discarded that single CO molecules underwent desorption (though there is evidence from studies of CO adsorption on Pd emitter planes that this may occur only to a negligible extent). This process would escape observation since Rh atoms or, possibly, Rh complex compounds and not CO molecules are visible in FIM. Even though adsorbate coverages remain uncertain during ion imaging, the general conclusion reached in this study is left unaltered. Accordingly, the morphological changes of the Rh particles are caused by a chemical reaction with adsorbed CO in the absence of an external electric field. This reaction is thermally activated: at 200 K the Rh atomic positions are unaffected by adsorbed CO; topographic changes are found to occur at 300 K and merge into a morphological reshaping of the crystals at 360 K (or higher, but still below the thermal desorption temperature of CO).

In contrast to FIM, the PFDMS method intentionally perturbs the ongoing reaction processes. Field desorption and evaporation by field pulses are destructive processes which clear away the adsorbed layer and provide a well-defined crystal surface at the beginning of each field-free reaction period. As discussed elsewhere (*19*), the correlation of ionic masses with neutral surface species is crucial for the interpretation of

the data. An important point in the present study is the occurrence of Rh-subcarbonyls, $Rh(CO)_x^{n+}$. The time dependence of the intensity of the dicarbonyl ion, $Rh(CO)_2^{2+}$, differs strongly from that of the $CO^+/RhCO^{2+}$ ions. Thus, field-induced association cannot be the determining process. There is also no evidence for the occurrence of adsorbed cluster compounds, $Rh_y(CO)_x$ (as might be suspected in view of the rich chemistry of polynuclear Rh carbonyls), so that a fragmentation process leading to di- and tricarbonyl species can be likewise dismissed. In an imaging atom-probe study on the same subject, Kellogg (*28*) concluded that the origin of CO^+ and $RhCO^{2+}$ was due to field fragmentation of neutral $Rh(CO)_3$. Rapidly rising field pulses were used in his study so that, indeed, fragmentation might have been important. In our study, the relatively long rise times of the pulses, 100–200 ns or more, make this process unlikely (ions leave the surface during ~0.1 ns so that they are no longer affected by further increasing field strengths).

In consideration of the above arguments we infer that a chemical surface reaction takes place in which adsorbed CO molecules are consecutively added to a single Rh (step) atom. Of course, the electric field may assist in this process and alter individual rate constants. A dc field strength variation would reveal this influence, but up to now such a measurement has only been performed in a study of Ru-subcarbonyl formation (which, however, should be quite similar to the Rh case). There, $Ru(CO)_x^{2+}$ species ($x \leq 4$) were detected with relative intensities strongly dependent on the dc field. In particular, it was found that increasing field strengths favoured the formation of low- rather than high-index species. The same trend of stabilities was obtained in a theoretical study by Wang and Kreuzer (*29*). It must be concluded from these studies that the surface reaction towards high-index subcarbonyls is impeded by dc fields. Furthermore,it is likely that the relative surface coverages of these species are altered during the course of field pulses with otherwise field-free reaction intervals. For this reason and with regard to the lack of knowledge of detailed field effects in Rh-subcarbonyl formation, we refrain from a calculation of respective surface coverages.

Mechanisms and Kinetics

In this section a microscopic model is set up which describes the initial reaction steps leading to the topographical and morphological changes observed in FIM. The experimental evidence for the model was obtained in PFDMS and is based on the knowledge of layer composition and kinetic data of reaction processes.

Adsorption of CO was found to take place with high initial sticking probabiliites, $S_0 = 0.85–0.95$. Both terrace sites and steps can be occupied. The former dominate the crystal surface and act as a gate for CO molecules impinging from the gas phase. Of course, direct adsorption at steps can also occur. However, occupation via surface diffusion is more likely.

$$CO_{gas} + [\ ]_{ad} \Leftrightarrow CO_{ad} \qquad (1a)$$

$$CO_{ad} + [\ ]_{step} \Leftrightarrow CO_{step} + [\ ]_{ad}. \qquad (1b)$$

A Rh-dicarbonyl species can be formed by addition of another CO_{ad} species to an occupied *step* site. CO_{ad} bound in multiple form to a single Rh *terrace* atom is not considered here since this binding mode has never been observed in vibrational spectroscopy of low-index Rh single crystal surfaces. The temperature dependence of $Rh(CO)_2^{2+}$ desorption suggests the formation of the respective neutral species to be thermally activated. It is most likely that this process is associated with Rh–Rh bond rupture in kink site positions:

$$(RhCO)_{kink} + CO_{ad} \Leftrightarrow Rh(CO)_{2.ad} + [\ ]_{kink}. \qquad (2)$$

The liberation of a $Rh(CO)_{2.ad}$ species is a repetitive process as long as kink sites are reproduced (usually, until an open chain of atoms is used up). This is illustrated in Fig.

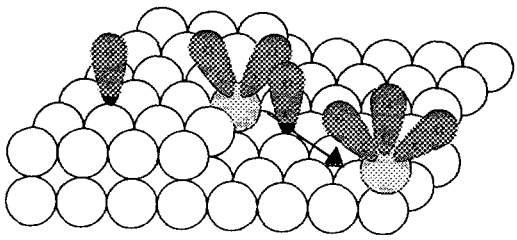

FIG. 11. Ball model to illustrate the continuous removal of Rh kink site atoms as subcarbonyls.

11. From an energetic point of view, $Rh(CO)_{2.ad}$ formation requires considerable effort. In fact, this is reflected by the rather long delay times of the order of milliseconds as measured in PFDMS. Once a $Rh(CO)_{2.ad}$ species is liberated, it may diffuse across the surface and, occasionally, react with another CO_{ad} to give $Rh(CO)_{3.ad}$. For the short reaction times, t_R, applied in PFDMS, the forward reaction of step (2) dominates. Thus, from the initial rise of the $Rh(CO)_2^{2+}$ intensities in Figs. 9 and 10 (and by taking into account ~20% transmission probability of the spectrometer) formation rates of 5×10^{-3} to 10^{-2} molecules per site per second at 298 K can be calculated. This takes for granted that (i) field effects as discussed above are negligible and (ii) diffusion does not alter the respective surface coverages in the monitored area. For the field strengths used during t_R variation, long-range diffusion from the shank towards the apex is effectively suppressed (for a more detailed argumentation, see Ref. (*19*)).

C–O bond rupture causing deposition of carbon and oxygen was also found to occur. There is experimental evidence that this process is quite easily accomplished at step sites (*21*, *24*). Thus, a competition with $Rh(CO)_2$ formation is suspected to exist. For the rather short time scale of PFDMS measurements only small amounts of carbon and oxygen are built up. We infer that dissociation is slower than association at temperatures up to at least 420 K, i.e., $Rh(CO)_2$ production dominates.

It seems clear from the above reaction mechanism that $Rh(CO)_{2.ad}$ liberation must lead to changes in the surface structure of Rh crystals. Our FIM studies have made visible these changes. In contrast to conditions in PFDMS, the reactions preceding ion imaging run to completion (the images remained nearly unchanged for higher CO gas pressures or longer reaction periods than used in the figures presented here). Of course, the reverse reaction, i.e., the decomposition of $Rh(CO)_{2.ad}$ in kink site positions comes into play when approaching equilibrium conditions. As a whole, rupture and deposition of Rh atoms in half-crystal sites will cause the build-up of facet structures with low-index terraces as observed in FIM. Carbon and oxygen atoms occasionally released during CO dissociation at steps, may block the restructuring of the surface so that irregular facets will be formed. In the absence of inhibition effects, one would expect the formation of regular polyhedrons with low-index planes in the facets of their slopes. Kink sites would only be present at the common edges of the slopes. Our FIM results have indeed shown that polyhedral crystal shapes are largely approached during reaction with CO at 360 or 420 K.

In summary of this section, it has been shown that Rh kink sites are intrinsically unstable in the presence of adsorbed CO. The kinetic constraints associated with their rupture can be overcome by mild heating. From a thermodynamic point of view, the formation of low-index planes during faceting of the crystals is favourable as the energetic stability of these planes overcompensates the increase of the surface area during restructuring.

Comparison with Literature

It seems worthwhile to put into more general perspective the findings of the present study and to point out the implications which they might have for understanding the reaction behavior of "more real" Rh catalysts.

The idea that field ion microscopy could make visible adsorption-induced structural changes of field emitter surfaces goes back to the early work of Holscher and Sachtler (*8*). These authors applied FIM to study CO adsorption on W field emitter tips. They concluded that the extra spots appearing in their field ion micrographs were due to metal atoms displaced from their original lattice sites rather than due to chemisorbed CO molecules as previously proposed by Ehrlich (*9*). Later work by others, however, called in question this interpretation and suspected much of what Holscher and Sachtler (*8*) attributed to adsorption-induced phenomena was in fact due to desorption during ion imaging. The present work has provided clear evidence for the occurrence of adsorbate-driven restructuring. Well-defined faceting was seen to occur during the reaction of CO with Rh field emitter particles ultimately leading to their reshaping from nearly hemispherical to polyhedral. Similarly strong morphological changes were up to now only observed by Schmidt *et al.* (*30*) in a study of CO on Ni field emitter crystals. These authors argued that individual Ni atoms may evaporate thermally in form of gaseous $Ni(CO)_4$ so that the crystal shapes evolve into a dissolution end-form. For thermodynamical reasons the formation of volatile Rh-carbonyls can be excluded in our study (much lower pressures here than those in Ref. (*30*)).

The chemical analysis by PFDMS of the adsorbed layer clearly identified $Rh^0(CO)_2$ as a (mobile) chemical component of the adsorbed layer. On the other hand, several IR studies with Rh/Al_2O_3 catalysts (*31–42*) indicated the occurrence of a gem-dicarbonyl with the Rh atom in the +1 oxidation state. According to the results of Basu *et al.* (*42*), hydroxyl groups of the support surface are directly involved in the formation process of $Rh^I(CO)_2$. Of course, this takes for granted that Rh–Rh bond rupture takes place in the surface of the particles. Experimental proof for a considerable disturbance of the Rh coordination number due to CO adsorption was obtained in EXAFS (extended X-ray absorption fine structure) studies (*39*). There, small Rh crystallites were seen to dissolve, ultimately leading to atomically dispersed Rh^I sites. Our PFDMS results provide a link to these studies in that they identify $Rh^0(CO)_{2,ad}$ to be the likely precursor species capable of migrating across the Rh/support interface and reacting with OH groups of the support surface:

$$Rh^0(CO)_{2,ad} + Al\text{–}OH \Rightarrow Al\text{–}O\text{–}Rh^I(CO)_2 + [\,]_{ad} + \tfrac{1}{2}H_2. \quad (3)$$

There is strong evidence from IR work of other authors (*32, 38*) that $Rh^I(CO)_2$ formation on Rh/Al_2O_3 occurs via an activated process. For example, Wang and Yates (*38*) found the characteristic doublet of $Rh^I(CO)_2$ absorbance to develop at temperatures above 200 K. For technical reasons, PFD mass spectra could not be taken at this low temperature. However, this and previous FIM work (*16*) have demonstrated that the onset for CO-induced topographic changes of Rh field emitter planes was near 240 K which coincides nicely with the temperature for $Rh^I(CO)_2$ occurrence given by Wang and Yates (*38*). The same authors have also provided IR data on the reversible formation of a $Rh^I(CO)_3$ species. According to our view, following the PFDMS results obtained here, $Rh^0(CO)_{3,ad}$ is produced in the terrace regions of the tip surface by addition of another CO_{ad} to the $Rh^0(CO)_{2,ad}$ precursor.

Equations (1)–(3) of our reaction model do not predict a dependence on the Rh particle size. Yet, there is ample evidence that $Rh^I(CO)_2$ IR detection necessitates high Rh dispersion. Only for sufficiently small particle sizes the characteristic doublet absorbance of $Rh^I(CO)_2$ was seen in the spectra (*31–42*). This, however, does not mean that dicarbonyl formation is prevented on large supported Rh particles. According to our view, the availability of Rh kink sites is an important prerequisite for the formation of $Rh^0(CO)_{2,ad}$. This assumption is appropriate for the experimental conditions present in PFDMS where concomitant field

evaporation of the substrate preserves the number density of kinks. During long-time reaction with CO, however, Rh particles undergo morphological changes accompanied by kink site annihilation and consequent loss of activity in dicarbonyl liberation. The absence of the $Rh^{I}(CO)_2$ IR absorbance in studies with large Rh-supported particles must mean that the reshaping process involving mobile $Rh^{0}(CO)_2$ is faster than the dissolution process causing $Rh^{I}(CO)_2$ formation. In fact, mild reaction conditions (temperatures at or above room temperature as well as CO pressures at or below 10^{-3} Pa) and rather short reaction times (some minutes) were found sufficient in our FIM studies to produce polyhedral crystal shapes. A recent study with transition electron microscopy (TEM) by Krause and Schmidt (*43*) was unable to observe CO-induced structural changes of Rh-supported particles with diameters of ~10 nm, possibly because of the limited resolution in TEM. However, the disruption of the particles with subsequent formation of $Rh^{I}(CO)_2$ was not seen either in their study. Instead, some sintering of adjacent particles was found to occur at room temperature as well as at 523 K. This is quite similar to the findings of Solymosi and Pásztor (*40*), according to which reductive agglomeration of mobile $Rh^{I}(CO)_2$ takes place at 448 K and above.

The FIM results of the present study may also contribute in answering the question why certain catalytic reactions are apparently sensitive to the structure of the catalyst surface whereas others are not. In particular, there is ample evidence from a number of studies (see, for example, (*44–46*)) that CO oxidation over noble metals is structure-insensitive in the CO inhibition regime (though experimental conditions can be adjusted for which self-sustained rate oscillations along with periodic changes of the surface structure can be established; see (*47*)). According to our FIM results, Rh as well as Pd emitter crystals (*23*) undergo restructuring whereby facets with densely packed planes are formed. We infer that inhomogeneities in the surface structure of Rh catalyst particles are likewise removed in the presence of adsorbed CO. This could mean that the oxidation reaction always takes place on rather smooth particle surfaces no matter which were the actual particle shapes before the catalytic run-in period. Future FIM studies will directly address CO oxidation over noble metal field emitter particles.

ACKNOWLEDGMENTS

Experiments by means of pulsed field desorption mass spectrometry were performed at the Fritz-Haber-Institut of the Max-Plack-Geselschaft in Berlin. We thank G. Abend and J. H. Block for stimulating discussions. One of us (A.G.) has been supported by the Swiss Nationalfonds, which is greatfully acknowledged. For corrections to the English language, thanks are due to D. Duff.

REFERENCES

1. Ganz, E., Sattler, K., and Clarke, J., *Surf. Sci.* **219,** 33 (1989).
2. Colchero, J., Marti, O., Mlynek, J., Humbert, A., Henry, C. R., and Chapon, C., *J. Vac. Sci. Technol. B* **9**(2), 794 (1991).
3. Müller, U., Sattler, K., Xhie, J., Venkateswaran, N., and Raina, G., *J. Vac. Sci. Technol. B* **9**(2), 829 (1991).
4. van de Leemput, L. E. C., Gerritsen, J. W., Rongen, P.H. H., Smokers, R. T. M., Wierenga, H. A., van Kempen, H., and Schmid, G., *J. Vac. Sci. Technol. B* **9**(2), 814 (1991).
5. Yeung, K. L., and Wolf, E. E., *J. Vac. Sci. Technol. A* **10**(4), 651 (1992).
6. Krause, K. R., and Schmidt, L. D., *Catal. Lett.* **14,** 141 (1992).
7. Smith, D.J., *Surf. Sci.* **178,** 462 (1986).
8. Holscher, A. A., and Sachtler, W.M. H., *Discuss. Faraday Soc.* **41,** 29 (1966).
9. Ehrlich, G., *Discuss. Faraday Soc.* **41,** 7 (1966).
10. Ehrlich, G., and Hudda, F. G., *Philos. Mag.* **8,** 1587 (1963).
11. Nishikawa, O., and Müller, E. W., *J. Appl. Phys.* **35,** 2806 (1964).
12. Bassett, D. W., *Br. J. Appl. Phys.* **18,** 1753 (1967).
13. Lewis, R. T., and Gomer, R., *Surf. Sci.* **26,** 197 (1971).
14. Brenner, S. S., and McKinney, J. T., *Surf. Sci.* **20,** 411 (1970).
15. Andrew, R., and Williams, E.M., *Surf. Sci.* **32,** 157 (1972).
16. Gaussmann, A., and Kruse, N., *Surf. Sci.* **266,** 46 (1992).
17. Kruse, N., and Gaussmann, A., *Surf. Sci.* **266,** 51 (1992).

18. Kruse, N., *Surf. Sci.* **178,** 820 (1986).
19. Kruse, N., Abend, G., and Block, J. H., *J. Chem. Phys.* **88**(2), 1307 (1987).
20. Chuah, G.-K., Kruse, N., Schmidt, W. A., Block, J. H., and Abend, G., *J. Catal.* **119,** 342 (1989).
21. Kruse, N., and Gaussmann, A., *Appl. Surf. Sci.* **67,** 160 (1993).
22. Block, J.H., *in* "Methods of Surface Analysis" (A. W. Czanderna, Ed.), Vol. 1, p. 379, Methods and Phenomena I: Their Applications in Science and Technology. Elsevier, Amsterdam, 1975.
23. Gaussmann, A., and Kruse, N., *Catal. Lett.* **10,** 305 (1991).
24. Rebholz, M., Prins, R., and Kruse, N., *Surf. Sci.* **259,** L797 (1991).
25. Kruse, N., *J. Vac. Sci. Technol. A* **8,** 3432 (1990).
26. Thiel, P. A., Williams, E. D., Yates, J. T., Jr., and Weinberg, W. H., *Surf. Sci.* **84,** 54 (1979).
27. Gaussmann, A., and Kruse, N., *Surf. Sci.* **279,** 319 (1992).
28. Kellogg, G. L., *J. Phys. (Paris)* **C6-48,** 233 (1987).
29. Wang, L. C., and Kreuzer, H. J., *J. Phys. (Paris)* **C8-53,** 50 (1989).
30. Schmidt, W. A., Block, J.H., and Becker, K. A., **122,** 409 (1982).
31. Yang, A. C., and Garland, C. W., *J. Phys. Chem.* **61,** 1504 (1957).
32. Primet, M. J., *J. Chem. Soc. Faraday Trans. I* **74,** 2570 (1978).
33. Yates, J. T., Jr., Duncan, T.M., Worley, S. D., and Vaughan, R. W., *J. Chem. Phys.* **71,** 3908 (1979).
34. Yates, D. J. C., Murrell, L.L., and Prestridge, E. B., *J. Catal.* **57,** 41 (1979).
35. Rice, C. A., Worley, S. D., Curtis, C. W., Guin, J. A., and Tarrer, A. R., *J. Chem. Phys.* **74,** 6487 (1981).
36. Cavanagh, R. R., and Yates, J. T., Jr., *J. Chem. Phys.* **74,** 4150 (1981).
37. Worley, S. D., Rice, C. A., Mattson, G. A., Curtis, C. W., Guin, J. A., and Tarrer, A. R., *J. Phys. Chem.* **86,** 2714 (1982).
38. Wang, H. P., and Yates, J. T., Jr., *J. Catal.* **89,** 79 (1984).
39. van't Blik, H. F. J., van Zon, J. B. A. D., Huizinga, T., Vis, J. C., Koningsberger, D. C., and Prins, R., *J. Phys. Chem.* **87,** 2264 (1983); *J. Am. Chem. Soc.* **107,** 3139 (1985).
40. Solymosi, F., and Pásztor, M., *J. Phys. Chem.* **89,** 4783 (1985).
41. Keyes, M. P., and Watters, K. L., *J. Catal.* **100,** 477 (1986).
42. Basu, P., Panayotov, D., and Yates, J. T., Jr., *J. Am. Chem. Soc.* **110,** 2074 (1988).
43. Krause, K. R., and Schmidt, D. L., *Catal. Lett.* **14,** 141 (1992).
44. Ertl, G., and Koch, J., *in* "Proceedings, 5th International Congress on Catalysis, Palm Beach, 1972" (J. W. Hightower, Ed.), p. 969. North-Holland, Amsterdam, 1973.
45. Ladas, S., Poppa, H., and Boudart, M., *Surf. Sci.* **102,** 151 (1981).
46. Oh, S. H., Fisher, G. B., Carpenter, J. E., and Goodman, D. W., *J. Catal.* **100,** 360 (1986).
47. Ertl, G., *Adv. Catal.* **37,** 213 (1990).